AIAA JOURNAL
Vol. 32, No. 9, September 1994

Visualized Flow Patterns of Double Concentric Jets at Low Annulus Velocities

Rong F. Huang* and Chih L. Lin†
National Taiwan Institute of Technology, Taipei, Taiwan 10672, Republic of China

The flow structures in the near wake region of the unducted double concentric jets at low Reynolds numbers are studied by smoke-wire flow visualization technique. Four typical characteristic flow regimes—weak flow, pre-penetration, transition, and penetration—are identified for different jet velocities in the near disk region. Flow patterns and behavior in each characteristic flow regime are investigated. The contours of the separation surfaces and the lengths of the recirculation zone in various flow regimes are correlated with nondimensional parameters. The recirculation length reaches a maximum in the transition region. The toroidal recirculation region exhibits both expelling and shear-layer vortex shedding. The shedding processes are presented, and the frequencies are correlated with Strouhal number and central-to-annular jet velocity ratio.

Nomenclature

D = diameter of circular disk, 20 mm
D_a = outer diameter of annular jet, 30 mm
D_c = exit diameter of central jet, 3.4 mm
f = frequency of vortex shedding, Hz
J_a = momentum flux of annular jet, $\rho_a u_a^2$
J_c = momentum flux of central jet, $\rho_c u_c^2$
L_r = axial length of recirculation zone
R = radius of circular disk, 10 mm
Re_a = Reynolds number of annular jet based on the disk diameter
Re_c = Reynolds number of central jet based on the central jet diameter
r = radial coordinate, originated from center of circular disk
St = Strouhal number, fD/u_a
u_a = average exit velocity of annular jet
u_c = average exit velocity of central jet
u_d = displacement velocity, $0.3u_c - u_a$
w_{max} = maximum half-width of the recirculation zone
Z = axial coordinate, originated from center of circular disk
ρ_a = mass density of annular flow
ρ_c = mass density of central jet

Introduction

DOUBLE concentric jets have been used in some engineering applications, e.g., nonpremixed bluff-body combustors,[1] chemical engineering, and cooling systems.[2] The flow structure of the double concentric jets has been extensively studied by investigators.[3–6] The mixing characteristics in a furnace and a cold model determined from measurements of gas concentrations and velocity distributions has been studied by Beér et al.[3] They proposed a similarity criterion, which was modified from Thring and Newby's formulation[7] for combusting coaxial jets, to scale up the mixing patterns in the model tests to the furnace applications. Chigier and Beér[4] have measured the mean velocity and static-pressure distributions in the region close to the exit of the nozzles of turbulent concentric jets with Reynolds numbers higher than 10^5. They found that the length of the recirculating toroidal vortex is essentially determined by the diameter of the disk and the velocity ratio whereas the pressure distributions are a function of the momentum flux of the central jet. At high central jet velocities, the stagnation points were no longer found on the centerline as in the case of low central jet velocities but were found at the points of impingement of the converging annular and the diverging central streamlines.

Roquemore et al.[5] introduced a two-dimensional sheet-lighting technique coupled with a fast chemically reacting system to visualize the turbulent mixing and the vortex shedding processes. They defined two stagnation points for flow conditions that the momentum of the reverse flowing annular air is larger than the momentum of the central jet and so that the central jet flow is turned back toward the bluff body. The centerline location, where the central jet is turned, was called the forward stagnation point. The maximum length of the recirculation zone along the centerline was called the aft stagnation point. When the momentum of the central jet is larger than the reverse flowing annular air, the central jet penetrates the recirculation zone and, hence, no stagnation points exist along the centerline. They postulated that the time average flowfields are similar when the ratio of central jet velocity to annular air velocity is constant. They classified the flow patterns into annular jet dominant, neither jet dominant, and central jet dominant regimes. For central-to-annular jet velocity ratios lower than 0.4, the momentum of the reverse annular flow is large enough to turn the central jet before it reaches the height of the time averaged center of the large recirculation zone. For central-to-annular jet velocity ratios between 0.4 and 1.5, the momentum of the central jet is sufficient to move the forward stagnation point above the axial height of the large vortex center. The tip of the central jet fluctuates unsteadily in this regime. For central-to-annular jet velocity ratios greater than 1.5, the central jet completely penetrates the recirculation zone and appears to entrain a large quantity of annular air. A large central jet entrainment rate reduces the size of the recirculation zone. They also found that for annulus velocities below 1 m/s the recirculation zone appears to be laminar. At annulus velocities between 1 m/s and 8 m/s, quasiperiodic spiral vortices are formed in the shear layer of the annular jet. For annulus velocities higher than 8 m/s, a notable change in the noise level occurs and high-frequency random vortex shedding is observed. The variations of the recirculation length in the near-wake region behind the axisymmetric bluff body already discussed follow an asymptotic behavior which was analytically derived by Li and Tankin.[6]

The flow patterns were basically classified according to the penetration of the center jet through the apex of the recirculation zone in the previously mentioned investigations. The key parameters dominating the flow characteristics are the central-to-annular jet velocity ratio and the blockage ratio.[5,6] The range of annulus Reynolds number in the previous studies covered from the order of 10^3–10^5. The flow phenomena in the range of annulus Reynolds number lower than 10^3 are still not clear. The studies of the double concentric jets at low annulus Reynolds numbers are important not only to help to understand the detailed phenomena and mechanism

Received Nov. 20, 1993; revision received April 15, 1994; accepted for publication April 15, 1994.

*Associate Professor, Department of Mechanical Engineering. Member AIAA.
†Graduate Student, Department of Mechanical Engineering.

of the interaction of the recirculation bubble and flushing jet, but are also important to applications of the nonpremixed type of burners for combustion processes which require a fuel-rich mixture at the flame front but a stoichiometric or lean mixing ratio farther downstream so that complete combustion is obtained within the combustion chamber.[3] Based on background knowledge from previous work on this subject, we set up a facility using twisted dual smoke-wire flow visualization technique to study the detailed flow patterns in the toroidal vortex and the dynamic behavior of the recirculation zone for flows in low annular jet velocity regime. This paper presents the results of the study on the characteristics of the flow modes, the recirculation length, and the vortex shedding.

Experimental Setup

The experiments are conducted with the setup shown in Fig. 1. The annular and central jets are continuously supplied by two separate flow systems consisting of centrifugal blowers, acoustical filters, pressure regulators, needle valves, and open-jet wind-tunnel assemblies. The acoustical filters are necessary here to flatten the ripples of the flow from the blowers.[8] The pressure regulators and the needle valves serve as the pressure stabilizers and the flow rate controllers, respectively.

The open-jet wind-tunnel assemblies are designed to function as the flow conditioning and measuring systems. The tunnels are circular in cross section. Four layers of No. 80 metallic screens are placed at the inlet of each tunnel to reduce the turbulence intensity of the flow in the test section. A section of plenum chamber is followed downstream to settle down the regulated homogeneous turbulence generated by the screens. A well-contoured nozzle with contraction ratio of 25 is fitted to the plenum chamber to accelerate the flow. The contour of the nozzle is well designed and machined according to Hussain and Ramjee's suggestion[9] to suppress the boundary-layer thickness so that the top-hat velocity profile is obtained at the exit of the nozzle. A circular disk with a 20 mm diameter and 0.5 mm thickness is placed concentrically at the exit of the 30-mm-diam cylindrical test section which is adapted to the exit of the nozzle. The blockage ratio of the disk on the annular jet defined by D^2/D_a^2 is 0.44. The central jet has an exit diameter of 3.4 mm. The wind-tunnel assemblies are surrounded by three layers of meshed screens to keep the test environment draft free.

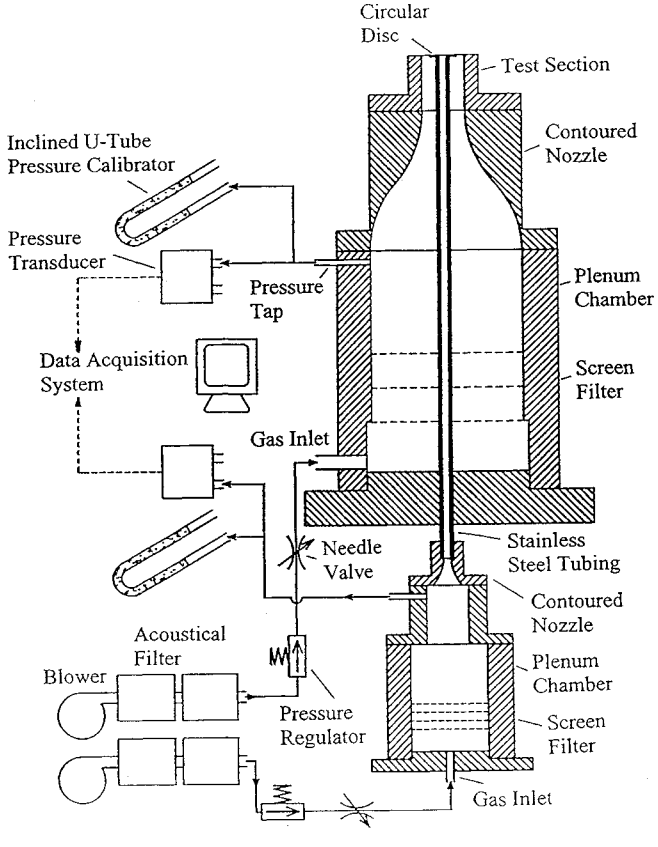

Fig. 1 Experimental setup.

The large contraction ratios of the nozzles ensure very slow motion in the plenum chambers so that the total pressures could be accurately measured from the pressure taps on the walls of the plenum chambers. The average exit velocities of the annular and central jets are calculated using the dynamic pressures which are the pressure differences between the total pressures measured at the plenum chambers and the atmospheric pressure. The dynamic pressures are measured with Validyne VR pressure transducers which are on-line calibrated with inclined U-tube micromanometers. The electronic output signals from the pressure transducer are fed to a PC-based data acquisition system to convert the raw data to the engineering units of pressures and average velocities. Before the experiments are conducted, the average velocity and turbulence intensity profiles of the central and annular jets across a $Z = 0.5$-mm plane are independently measured by a one-component hot-wire anemometer. The exit velocity profile of the central jet at an average velocity of 1.5 m/s is fully developed. The exit velocity profile of the annular jet at an average velocity of 0.9 m/s has a sharp radial velocity gradient of about 1000 (1/s) at the edge of disk, whereas the radial velocity gradient at the outer edge of the annular flow is only 200 (1/s). Since the exiting annular velocity profile may have profound effect on the jet instability properties, say, frequency and intensity of the vortex shedding developed from the shear-layer instability wave, care must be taken when comparing all instability properties of separated flows. The turbulence intensities are less than 0.5% in the experimental range of this work.

A stainless steel wire with a 100 μm diameter wound around by another one to form a twisted dual wire is placed across the center plane of the jets at $Z = 1$ mm. Thin mineral oil is brush coated on the wire surface and is ohmically heated to generate fine smoke streaks to make the flowfield observable. The smoke streaks are 0.7 mm in width, and the space between each smoke streak is controlled within 0.3 mm. The observable smoke streaks generated by this configuration at $u_a = 1$ m/s ($Re_a = 1295$) can last for at least 90 s. The Reynolds number based on the smoke-wire diameter in this study is kept lower than 16, which is less than the limit of 20, recommended by Mueller,[10] to avoid commencement of vortex shedding behind the wire. The surface temperature of the smoke wire is kept as low as possible but still high enough to evaporate the oil so that the buoyancy-induced convection[11] is estimated to be below 2.5 cm/s. The diameter of the condensed vapor aerosols (the smoke) of the thin mineral oil are commonly at the order of 1 μm according to Batill and Mueller.[12] Hence, the slip factor[13] for these aerosols is about 1.168. The relaxation time and the deviated particle path from a streamline turning in a 90-deg angle are estimated to be about 65 μs and 65 μm, respectively, at $u_a = 1$ m/s. Thus, the Stokes number[13] based on the diameter of the circular disk is 0.003, which is much smaller than unity. Therefore, the smoke streaks are considered to follow the flow properly.

Results and Discussion

Flow Patterns

Weak Flow Region

The domain of the annular-central jet velocities in Fig. 2 can be classified into four main regions according to the characteristic flow patterns. Region I is called the weak flow region. In this region the jet velocities are not high enough to form a closed toroidal recirculation bubble. Subregions I(A), I(B), and I(C) in Fig. 2 correspond to the typical patterns, vortex free, Q tip, and open-top toroid, respectively. The typical vortex-free flow pattern in subregion I(A) is shown in Fig. 3a. Since the annular jet velocity is very low, the subatmospheric pressure in the near wake region is not low enough to cause reversal of the separation surface. Also, the central jet velocity in this subregion is not high enough to induce a near disk vortex as was found by Chigier and Beér.[4] The smoke streaks on both exits of central and annular jets go downstream without reversal. No trace of vortex structure is found in this subregion. Figure 3b shows the typical Q-tip pattern for flows in subregion I(B).

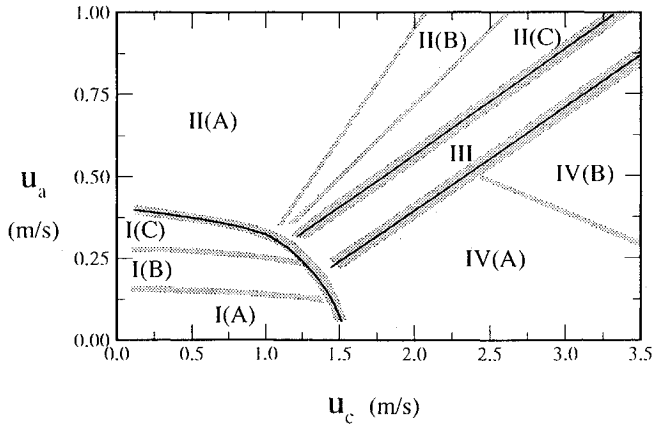

Fig. 2 Regions of the characteristic flow modes in velocity domain: region I, weak flow region; region II, prepenetration region; region III, transition region; and region IV, penetration region.

The subatmospheric pressure in the near wake region due to the increase of the annular jet velocity is now lower than that in subregion I(A) and, hence, causes the separation surface emanating from the edge of the disk to move toward the symmetric axis in the downstream area. A Q-tip flow pattern is formed. The Q-tip flow pattern, characterized by an axial flow reversal near the axis, resembles the meridional flow derived by Sullivan[14] for a flowfield with pressure gradients in r and Z directions set up by axisymmetric rotation of flow above a solid wall. Sullivan's solution illustrates the fact that low pressure in the core region near the wall can cause the reversal of the axial flow. The head of the Q tip is lifted by the central jet. The fluids of the central jet are radially deflected by the reverse flow and go downstream along the boundary of the Q tip so as to make the pattern visible. As the annular jet velocity is increased to subregion I(C), the pressure in the head area of the Q tip is low enough to form appreciable vorticity to entrain the deflected central jet fluid. The entrained fluids enlarge the size of the head of the Q tip and the smoke particles make the vortex visible as shown in Fig. 3c. The separation surface in this subregion is still not reversed and, hence, the flow pattern in this subregion is called open-top toroid. Increase in annular jet velocity will intensify the vorticity and enlarge the head area of the Q tip.

Prepenetration, Transition, and Penetration Regions

Regions II, III, and IV in Fig. 2 are called prepenetration, transition, and penetration regions, respectively. The terms adopted here originated from those employed by Chin and Tankin[15] for identification of vortical structures in a two-dimensional vertical bluff-body combustor. A displacement velocity u_d, defined by

$$u_d = 0.3u_c - u_a \tag{1}$$

can be used to classify the regions. The flow is in the prepenetration region if the value of u_d is negative. For $0 < u_d < 0.2$ m/s, the flow is in the transition region. The flow is in the penetration region when $u_d > 0.2$ m/s.

In region II of Fig. 2, the so-called prepenetration region, the momentum of the central jet is not high enough to overcome the momentum of the reverse flow of the recirculated fluids so that the flow patterns are characterized by the relative intensity of the central jet to the reverse flow. When flow conditions are in region II(A) of Fig. 2, the inner vortex expands outward to merge with the separation surface, which is curved inward. The recirculation bubble is formed, and the structure is quite unstable as shown in Fig. 3d. In this subregion, the momentum of the central jet is not strong enough to maintain an up-right jet column so that the vortex in the recirculation bubble takes certain preferential radial direction. This is probably caused by the Coanda effect.[16] The typical flow pattern in region II(B) is shown in Fig. 3e. In this region, the central jet has enough momentum to maintain a stable up-right column so that clear vortex structures are built up in the recirculation bubble due to the momentum balance of the central jet and the reverse flow. Defined by Roquemore et al.,[5] the forward stagnation point is the balance point of the central jet and the reverse flow whereas the aft stagnation point is the merge point of the separation surface to the center axis. These two stagnation points, as well as a pair of counter-rotating large vortex rings, characterize the flow patterns in this subregion. The upper vortex ring surrounds the Z axis, and the lower vortex ring surrounds the central jet column. The position of the forward stagnation point and the size of the vortices depend on the relative strength of the central jet and the reverse flow. The forward stagnation point moves downstream, the upper vortex ring shrinks, and the lower vortex ring enlarges as the central jet velocity is increased. For flows in region II(C), as shown in Fig. 3f, the upper vortex ring is pushed outward by the central jet. A large vortex ring surrounding the central column and a small vortex ring in the top area of the recirculation bubble are formed.

In region III as shown in Fig. 2, the flow patterns are transitional. The central jet is penetrating the apex of the reversed separation surface. During the transition process, the flow is very unstable and chaotic as shown in Fig. 3g. The rotation, engulfment, and distortion of the vortices are observed in the video tapes. It seems that violent random motions and energy exchange processes in the recirculation bubble are induced by the interaction of central jet and vortex structure in order to overcome the maximum pressure around the aft stagnation point.[3]

Region IV in Fig. 2 is for penetration flow patterns. As the central jet just penetrates the recirculation apex, the flowfield is stabilized. Figures 3h and 3i show the typical flow patterns in subregions IV(A) and IV(B), respectively. In subregion IV(A), the separation surface is not reversed. While in subregion IV(B), due to the lower pressure induced by the higher annular jet velocity, the separation surface is reversed to form the outer boundary of the recirculation bubble. In both subregions, a pair of counter-rotating vortex rings is formed. The upper vortex ring exists due to the pressure gradient and the momentum inertial as does that in region II. The lower vortex ring is induced by shear effect of the high-speed central jet. Figure 4 shows the typical flow pattern in this shear effect dominant region. The size of the upper vortex ring shrinks, and the intensity of the lower vortex ring increases with the increase of central jet velocity. A large amount of annular jet fluids is merged to and entrained by the central jet; afterward, the

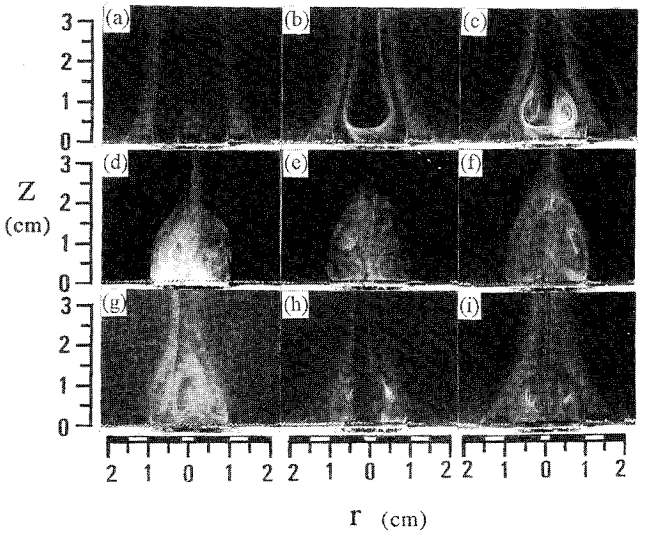

Fig. 3 Typical flow patterns correspond to characteristic flow regions in Fig. 2: a) I(A), u_a = 0.10 m/s, u_c = 1.05 m/s; b) I(B), u_a = 0.30 m/s, u_c = 1.11 m/s; c) I(C), u_a = 0.37 m/s, u_c = 1.11 m/s; d) II(A), u_a = 0.43 m/s, u_c = 1.09 m/s; e) II(B), u_a = 0.75 m/s, u_c = 1.79 m/s; f) II(C), u_a = 0.56 m/s, u_c = 2.03 m/s; g) III, u_a = 0.32 m/s, u_c = 1.52 m/s; h) IV(A), u_a = 0.30 m/s, u_c = 1.79 m/s; and i) IV(B), u_a = 0.47 m/s, u_c = 2.96 m/s.

combined jet convects downstream. This observation confirms the measurements of Chigier and Beér[4] which showed that at high central jet velocities the vortex center of the vortex ring resides around the root area and surrounds the central jet column, additionally, the stagnation point locates at a little higher position.

Separation Surface and Recirculation Length

The typical normalized contours of the free separation surface in characteristic flow regions II(B), II(C), III, and IV(B) are shown in Fig. 5. The contour in prepenetration region II(B) in Fig. 5 shows that the separation surface from the edge of the circular disk expands outward first and curves inward successively. At a certain height, the separation surface turns back to the upstream direction and merges with the axisymmetric axis at the saddle point to form the closed toroid. The turning and the saddle points shift toward the downstream direction with the increase of annular or central jet velocity, and eventually exhibit the typical contour of region II(C), shown in Fig. 5. When the flow conditions are in transition region III where the central jet is penetrating the apex of the closed toroid, the free separation surface goes downstream without reversal. The separation surfaces in regions I(A), I(B), I(C), and IV(A) which are not shown in Fig. 5 are also not reversed. The typical contour of separation surface in penetration region IV(B) shown in Fig. 5 turns at a lower position toward the central jet column and is reversed to form a vortex ring. The turning point moves upstream as the central jet velocity is increased. The contours of the separation surfaces with reversals correlated by using dimensionless groups Z/L_r and r/w_{max} collapse to a compact band as shown in Fig. 6, except for the reversed parts of the central jet dominant flow with very high central-to-annular jet momentum ratios. The recirculation length L_r is defined as the distance from the circular disk to the intersection of the Z axis and the asymptotic extension of the reversed separation surface from the turning point. The effects of Reynolds number on the non-dimensional correlation using Z/L_r and r/w_{max} are not appreciable in the low annulus velocity regime of this work. For the high annulus Reynolds number regime, however, although the contour and length of the recirculation bubble are primarily influenced by the blockage ratio and forebody geometry,[17] this correlation may have appreciable variation.

The variation of the recirculation lengths with central jet velocities at various annular jet velocities is shown in Fig. 7. According to the analysis of Li and Tankin,[6] the recirculation length should increase at low Re_a, decrease after a critical Re_a about 2000, and approach a constant at high Re_a for flows with zero central jet velocity. In this study, in which the values of Re_a are lower than 1200, the recirculation length increases with the increase of annular jet velocity for fixed central jet velocity. The recirculation length decreases with the increase of central jet velocity in prepenetration region II(A). In this region, the fluids of the central jet have neither enough momentum nor coherency to maintain an upright jet column and thus are absorbed by the annulus fluids via violent chaotic motions as shown in Fig. 3d. The energy is consumed inside the recirculation toroid and, consequently, according to the conservation law of momentum,[4] the recirculation length is reduced. As the flow conditions are in the prepenetration regions II(B) and II(C), the organized vortex structures are set up. The lower vortex ring enlarges as the central jet velocity is increased.

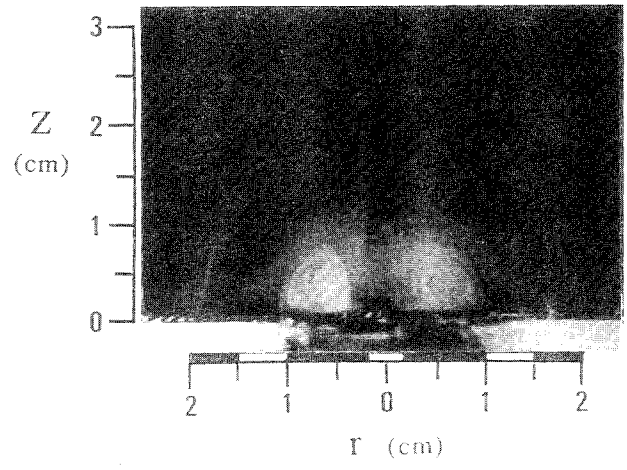

Fig. 4 Typical flow pattern at very high central-to-annular jet velocity ratio with u_a = 0.44 m/s and u_c = 7.84 m/s.

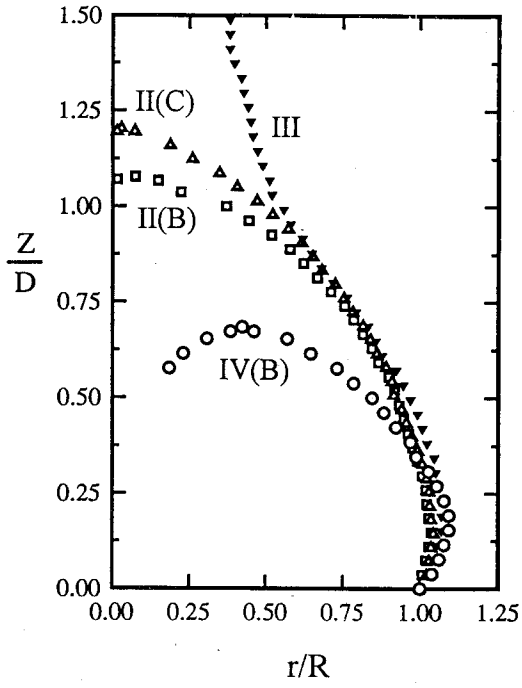

Fig. 5 Variation of contours of separation surfaces in different characteristic flow regions: II(B), u_a = 0.75 m/s, u_c = 1.79 m/s; II(C), u_a = 0.56 m/s, u_c = 2.03 m/s; III, u_a = 0.32 m/s, u_c = 1.52 m/s; and IV(B), u_a = 0.47 m/s, u_c = 2.96 m/s.

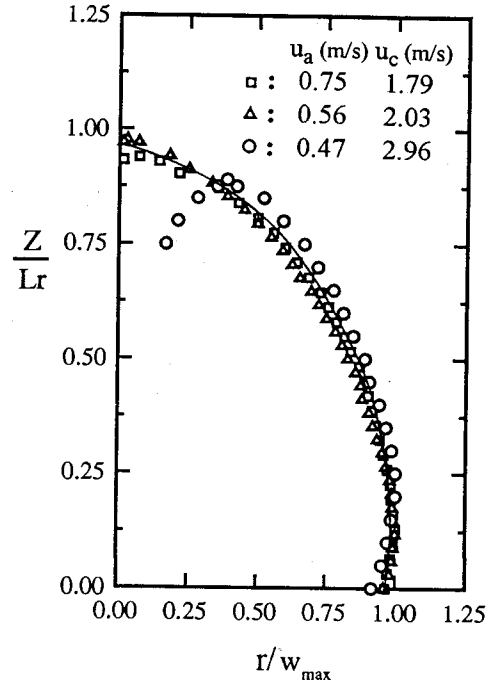

Fig. 6 Correlation of contours of reversed separation surfaces.

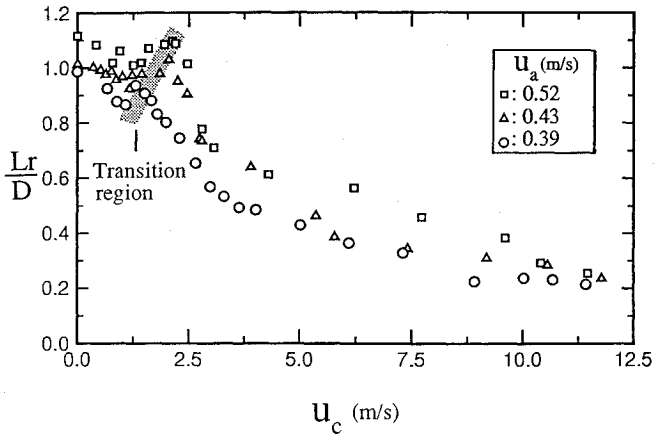

Fig. 7 Variation of recirculation length with central jet velocity at various annulus velocities.

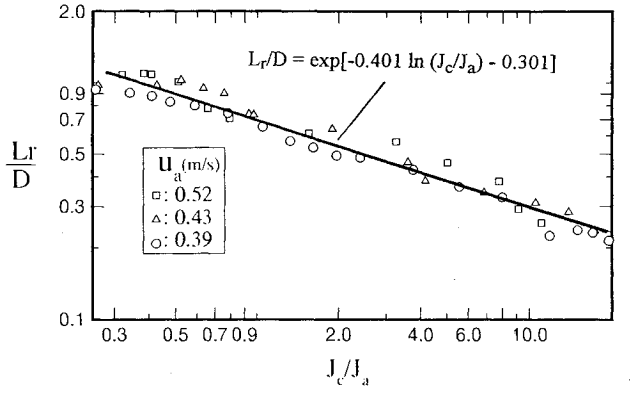

Fig. 8 Correlation of recirculation length.

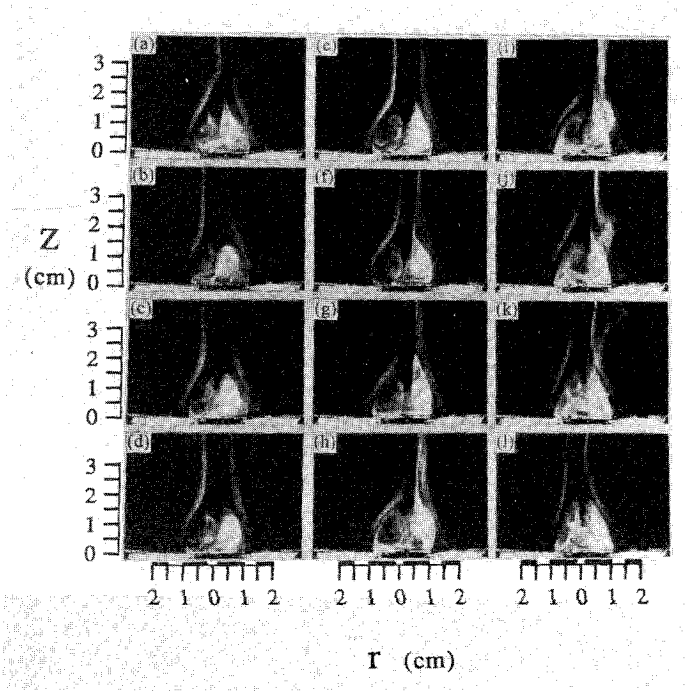

Fig. 9 Histogram of expelling shedding (mode 1) with u_a = 0.32 m/s and u_c = 1.14 m/s; time interval between each frame is 0.067 s and shedding frequency is 1.25 Hz.

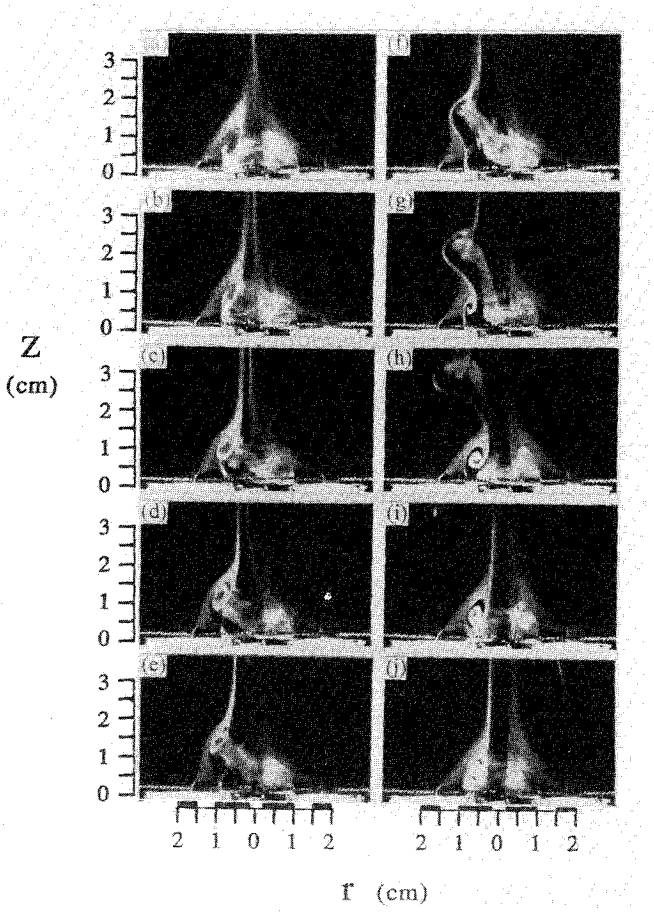

Fig. 10 Histogram of expelling shedding (mode 2) with u_a = 0.39 m/s and u_c = 5.02 m/s; time interval between each frame is 0.03 s and shedding frequency is 3.33 Hz.

The recirculation length thus increases with the increase of the central jet fluids. The recirculation length reaches its maximum in the transition region (III) where the central jet is penetrating through the apex of the closed toroid. After the penetration, the entrainment and momentum effects of the high-velocity central jet cause the shrinkage of the upper vortex ring as has been shown in Figs. 3h and 3i. Hence, the recirculation length in region IV(B) decreases with the increase of central jet velocity. The recirculation lengths in various regions are correlated logarithmically with central-to-annular jet momentum flux ratios by

$$L_r/D = \exp[-0.401\ \ell_n (J_c/J_a) - 0.301] \qquad (2)$$

The correlated results are shown in Fig. 8. The use of this correlation is for the convenient estimation of the recirculation length, rather than for examination of the precise variation of recirculation length in the regime of low central-to-annular jet momentum flux ratios. Again, the adequacy of extension of this correlation to high annulus Reynolds number regime is still unknown.

Shedding of Vortices

Expelling Shedding

Two types of vortex shedding are found in this experiment: expelling and shear-layer vortex shedding. As vorticity accumulated in the recirculation zone reaches a status of nonequilibrium, the redundant vorticity must be expelled in certain ways to keep equilibrium. Expelling vortex shedding is found in three basic modes. Mode 1 of expelling vortex shedding shown in the streak pictures Figs. 9a–9l is commonly observed in regions with low central jet velocities. Under some nonequilibrium conditions, the vortex enclosed in the open top separation surface in Fig. 9a becomes unsta-

ble and is stretched upward as shown in Figs. 9b–9h. Some fluids in the stretched vortex are then expelled away as shown in Figs. 9i–9l. Modes 2 and 3 of expelling shedding are observed in regions with high central jet velocities. The streak pictures in Fig. 10 show the evolution of the expelling shedding of mode 2. A vortex ring is stretched out of the left recirculation vortex in Fig. 10a. The stretching evolves in an asymmetric way as shown in Figs. 10b–10f. A small vortex is then induced from the left edge of the circular disk and grows when the vortex ring is expelled away, which is shown in Figs. 10g–10i. As the vortex ring is expelled, the newly induced vortex becomes stable and the whole vortex system resets to the initial condition as shown in Fig. 10j. The evolution of the expelling shedding of mode 3 is shown in Figs. 11a–11h. The trace of the expelling process is observable, though it is not very clear due to the high velocity of the central jet. The ring vortex surrounding the central jet column at the open top of the recirculation toroid is expelled downstream intermittently. It is probably induced from the high shear between the central jet and the reversed separation surface of the annular flow.

The frequency variation of the expelling shedding in various flow regions characterized by Strouhal number and central-to-annular jet velocity ratio is shown in Fig. 12a. The Strouhal number of the expelling shedding of mode 1 decreases with the increase of central-to-annular jet velocity in the prepenetration and transition regions. On the boundary of the transition and penetration regions, the shedding frequency reduces to almost zero. It seems that the central jet has the effect of prohibiting expelling shedding from the recirculating toroid before it penetrates the top of the toroid. In the penetration region, the frequency of expelling shedding of mode 2 increases with central jet velocity. The Strouhal number reaches a maximum of about 0.017 at a central-to-annular jet velocity ratio of 13. Further increase in central jet velocity will reduce the shedding frequency. The expelling shedding of mode 3 is commonly observed for a central-to-annular jet velocity ratio higher than 13. The shedding is not found when central-to-annular jet velocity ratio is higher than 28.

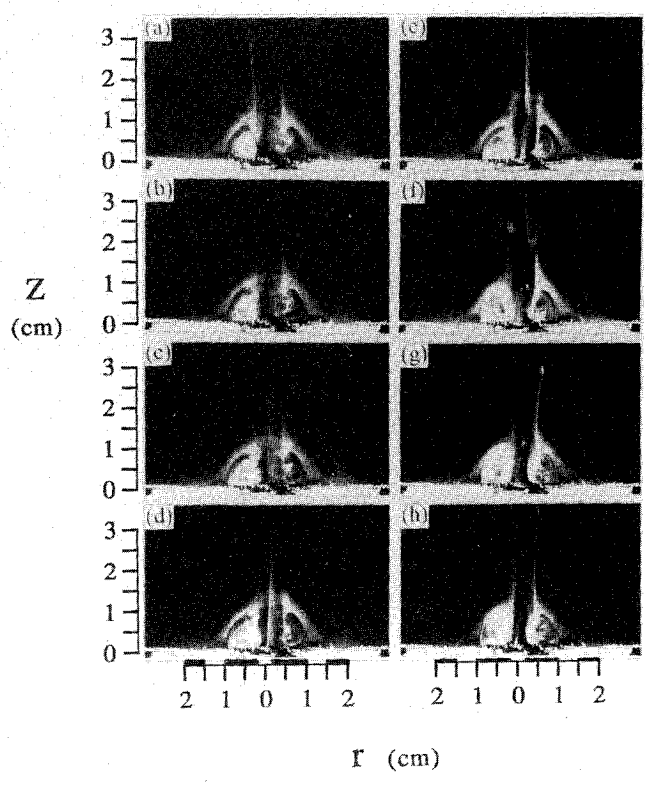

Fig. 11 Histogram of expelling shedding (mode 3) with u_a = 0.32 m/s and u_c = 5.44 m/s; time interval between each frame is 0.03 s and shedding frequency is 4.17 Hz.

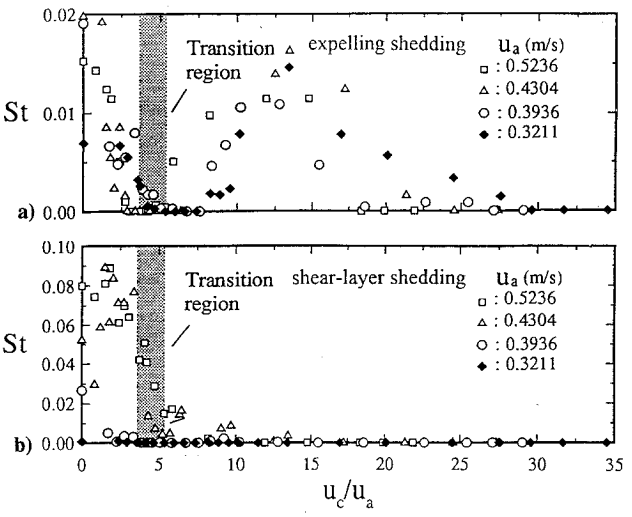

Fig. 12 Variation of Strouhal number of vortex shedding with central-to-annular jet velocity ratio: a) expelling shedding and b) shear-layer shedding.

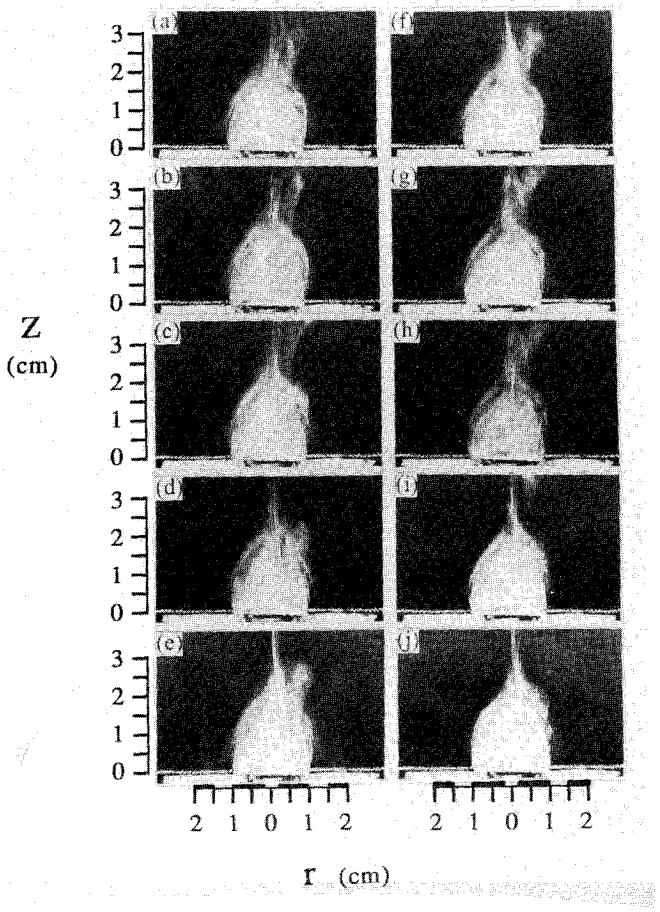

Fig. 13 Histogram of shear-layer shedding with u_a = 0.43 m/s and u_c = 1.17 m/s; time interval between each frame is 0.03 s and shedding frequency is 5.0 Hz.

Shear-Layer Shedding

The shear-layer vortex shedding is found only in the prepenetration and transition regions. The typical shedding process is shown in streak photographs, Figs. 13a–13j. A small vortex is first developed on the right shear layer boundary of the separation surface in Fig. 13a. It moves downstream and grows as seen in Figs. 13b and 13c. As it moves almost to the top of the toroid, the shedding starts

as shown in Fig. 13d. The vortex stretches downstream and eventually departs from the separation surface as shown in Figs. 13e–13j. The shear-layer shedding has higher maximum frequency compared to expelling shedding. The variation of Strouhal number with central-to-annular jet velocity is shown in Fig. 12b. The shedding frequency increases with central jet velocity in region II(A) and then decreases in regions II(B), II(C), and III. The maximum Strouhal number is about 0.09. In region II(A), the separation surface is not reversed, and the shear effect on the boundary increases with the increase of jet velocity ratio. As the flow is in regions II(B), II(C), and III, the boundary moves outward with the increase of central jet velocity as shown in Fig. 5. The shear effect on the boundary is decreased and so is the shedding frequency. The periodical shedding of the shear-layer vortex occurs differently from that found either in a two-dimensional mixing-layer or a wake in which the vortices are alternatively shed.

Concluding Remarks

The flow structures in the near wake region of the unducted double concentric jets at low Reynolds numbers are studied by smoke-wire flow-visualization technique. Four typical characteristic flow regimes: weak flow, prepenetration, transition, and penetration, are identified for different jet velocities in the near disk region. In weak flow region, the annular jet velocity is not high enough to cause reversal of separation surface. Three typical patterns, vortex free, Q tip, and open top toroid, are found in weak flow region. In the prepenetration region the structure of the toroidal vortex is categorized into three typical flow patterns according to the central-to-annular jet velocity ratios. Stable vortex structure is observed only when the central jet momentum is strong enough to maintain an up-right column. The structure is unsteady when the central jet is penetrating through the apex of the recirculation toroid in the transition region. In the penetration region, the high central jet momentum dominates the flowfield, additionally, three typical flow patterns are found. The contours of the reversed separation surfaces in various regions are correlated with non-dimensional parameters. The recirculation length reaches a maximum in the transition region. The recirculation length is logarithmically correlated by central-to-annular jet momentum ratio. The toroidal vortex exhibits both expelling and shear-layer vortex shedding. The shedding processes are presented and the frequencies are correlated with Strouhal number and central-to-annular jet velocity ratio.

References

[1]Reed, R. J., *North American Combustion Handbook*, 2nd ed., North American Manufacturing Co., Cleveland, OH, 1983, pp. 230–251.

[2]Aly, M. S., and Rashed, M. I. I., "Study of Double Concentric Jets with Different Geometric Configurations," *Journal of Wind Engineering and Industrial Aerodynamics*, Vol. 45, No. 1, 1992, pp. 1–10.

[3]Beér, J. M., Chigier, N. A., and Lee, K. B., "Modeling of Double Concentric Burning Jets," *Ninth Symposium (International) on Combustion*, The Combustion Institute, Academic Press, New York, 1963, pp. 892–900.

[4]Chigier, N. A., and Beér, J. M., "The Flow Region Near the Nozzle in Double Concentric Jets," *Journal of Basic Engineering*, Dec. 1964, pp. 797–804.

[5]Roquemore, W. M., Tankin, R. S., Chiu, H. H., and Lottes, S. A., "A Study of a Bluff-Body Combustor Using Laser Sheet Lighting," *Experiments in Fluids*, Vol. 4, No. 4, 1986, pp. 205–213.

[6]Li, X., and Tankin, R. S., "A Study of Cold and Combusting Flow Around Bluff-Body Combustors," *Combustion Science and Technology*, Vol. 52, No. 4, 1987, pp. 173–206.

[7]Thring, M. W., and Newby, M. P., "Combustion Length of Enclosed Turbulent Jet Flames," *Fourth Symposium (International) on Combustion*, The Combustion Institute, Williams and Wilkins, Baltimore, MD, 1953, pp. 789–796.

[8]Davis, D. D., Jr., "Acoustical Filters and Mufflers," *Handbook of Noise Control*, 1st ed., edited by C. M. Harris, McGraw-Hill, New York, 1957, pp. 21.2–21.44.

[9]Hussain, A. K. M. F., and Ramjee, V., "Effects of the Axisymmetric Contraction Shape on Incompressible Turbulent Flow," *Journal of Fluids Engineering*, Vol. 98, No. 1, 1976, pp. 58–69.

[10]Mueller T. J., "Flow Visualization by Direct Injection," *Fluid Mechanics Measurements*, 1st ed., edited by R. J. Goldstein, Hemisphere, New York, 1983, pp. 307–340.

[11]Bejan, A., *Convection Heat Transfer*, Wiley, New York, 1984, pp. 110–114.

[12]Batill, S. M., and Mueller, T. J., "Visualization of Transition in the Flow over an Airfoil Using the Smoke-Wire Technique," *AIAA Journal*, Vol. 19, No. 3, 1981, pp. 340–345.

[13]Flagan, R. C., and Seinfeld, J. H., *Fundamentals of Air Pollution Engineering*, Prentice Hall, Englewood Cliffs, NJ, 1988, pp. 295–307.

[14]Sullivan, R. D., "A Two-cell Vortex Solution of the Navier-Stokes Equations," *Journal of Aeronautical Science*, Vol. 26, No. 11, 1959, pp. 767–780.

[15]Chin, L. P., and Tankin, R. S., "Vortical Structures in a 2-D Vertical Bluff-Body Burner," *Combustion Science and Technology*, Vol. 80, No. 5, 1991, pp. 207–229.

[16]Tritton, D. J., *Physical Fluid Dynamics*, Oxford Univ. Press, New York, 1988, pp. 150–152.

[17]Beér, J. M., and Chigier, N. A., *Combustion Aerodynamics*, Robert E. Krieger, Malabar, FL, 1983, pp. 73–76.